Journal of Applied Polymer Science

Latex co-coagulation approach to fabrication of polyurethane/graphene nanocomposites with improved electrical conductivity, thermal conductivity, and barrier property

Sheng Li Wu,[1,2] Tie Jun Shi,[1] Li Yuan Zhang[3]

[1]School of Chemistry and Chemical Engineering, Hefei University of Technology, Hefei, Anhui 230009, People's Republic of China
[2]Anhui Institute for Food and Drug Control, Hefei, Anhui 230051, People's Republic of China
[3]Department of Chemistry and Environmental Engineering, Bengbu College, Bengbu, Anhui 233000, People's Republic of China
Correspondence to: T. J. Shi (E-mail: stjhfut@163.com)

ABSTRACT: This study describes a simple and effective method of synthesis of a polyurethane/graphene nanocomposite. Cationic waterborne polyurethane (CWPU) was used as the polymer matrix, and graphene oxide (GO) as a starting nanofiller. The CWPU/GO nanocomposite was prepared by first mixing a CWPU emulsion with a GO colloidal dispersion. The positively charged CWPU latex particles were assembled on the surfaces of the negatively charged GO nanoplatelets through electrostatic interactions. Then, the CWPU/chemically reduced GO (RGO) was obtained by treating the CWPU/GO with hydrazine hydrate in DMF. The results of X-ray diffraction (XRD), transmission electron microscopy (TEM), scanning electron microscopy (SEM), and Raman analysis showed that the RGO nanoplatelets were well dispersed and exfoliated in the CWPU matrix. The electrical conductivity of the CWPU/RGO nanocomposite could reach 0.28 S m^{-1}, and the thermal conductivity was as high as 1.71 W m^{-1} K^{-1}. The oxygen transmission rate (OTR) of the CWPU/RGO-coated PET film was significantly decreased to 0.6 cm^3 m^{-2} day^{-1}, indicating a high oxygen barrier property. This remarkable improvement in the electrical and thermal conductivity and barrier property of the CWPU/RGO nanocomposite is attributed to the electrostatic interactions and the molecular-level dispersion of RGO nanoplatelets in the CWPU matrix. © 2015 Wiley Periodicals, Inc. J. Appl. Polym. Sci. **2016**, *133*, 43117.

KEYWORDS: composites; graphene and fullerenes; polyurethanes; surfaces and interfaces; synthesis and processing

Received 2 July 2015; accepted 31 October 2015
DOI: 10.1002/app.43117

INTRODUCTION

Polyurethane (PU) is a flexible and elastic polymer synthesized by the reaction of diisocyanates with diols and widely used in coatings, adhesives, sealants, thermoplastic elastomers, and medical devices.[1] Nanotechnology is considered as a new approach to developing next-generation PU materials for broader industrial applications, with nanomaterials showing a strong ability to comprehensively upgrade the physical properties of PU materials for improved thermal, mechanical, and electrical properties of nanocomposites.[2–4] Graphene, a one-atom-thick two-dimensional basal plane of graphite, has attracted considerable attention because of its high mechanical properties (~1000 GPa), electrical conductivity (~6000 S cm^{-1}), thermal conductivity (~5000 W m^{-1} K^{-1}), surface area (2630 m^2 g^{-1}), and gas impermeability.[5–10] Recently, PU/graphene nanocomposites have been widely reported to enhance the electrical and thermal conductivity in polymeric systems.[11,12] Moreover, the lamellar structure of graphene makes it quite interesting as an alternative to the use of organ clay fillers to enhance the gas barrier properties of PU materials.[13,14] However, pristine graphene tends to form irreversible agglomerates through van der Waals interactions, leading to poor dispersion of graphene sheets in the polymer matrix. Moreover, the structure of graphene is atomically smooth and lacks interfacial bonding, which limits load transfer from the polymer matrix to the grapheme,[15] resulting in the poor performance of graphene/polymer nanocomposites. To understand this problem, functionalized graphene nanoplatelets (F-GNS) with special surface properties have been designed. By functionalizing the graphene surface, the interfacial interaction between the graphene and the polymer can be improved, and well-dispersed graphene nanocomposites can be successfully obtained. Popular chemically functionalized graphene includes graphene oxide (GO), reduced graphene oxide (RGO), and

Additional Supporting Information may be found in the online version of this article.

graphene with covalent or non-covalent surface modified through small molecules or polymers.[16–20] In addition, several strategies for preparing PU/graphene nanocomposites have been adopted to improve the dispersibility of the graphene sheets in the PU matrix, such as *in situ* polymerization,[21–24] melt blending,[25,26] and solution processing.[27–30] Melt blending is a versatile and commonly used method of fabricating polymeric materials, especially thermoplastic polymers. However, a drawback of this technique is that it may cause graphene buckling, and even rolling or shortening, due to strong shear forces, as evidenced by a rather high percolation threshold of electrical conductivity. In solution processing, graphene nanoplatelets are generally dispersed in a solvent and then mixed with a polymer solution by mechanical mixing or high-energy sonication. Although solution processing is considered as an effective means of preparing composites with good dispersion and exfoliation, the use of a solvent poses an add-on cost and contributes to environmental pollution. *In situ* polymerization is the most effective way of improving the dispersion and exfoliation of graphene in a matrix and can create a covalent bonding interface between graphene and the matrix; however, the polymerization process is usually accompanied by a viscosity increase that hinders manipulation and limits the load fraction. To resolve these issues, Piotr Król *et al.*[31,32] reported that the multistep method of synthesis of the polyurethane cationomer was allowed at the stage of synthesis of the isocyanate prepolymer to introduce graphene in the form of a suspension in tetrahydrofuran (THF) to prepare PU/graphene nanocomposites.

The latex co-coagulation method involves mixing the latex with other lattices or fillers, after which the polymer mixtures can be co-precipitated by adding flocculants. This method has been used in the fabrication of carbon nanotubes and clay-based polymer composites.[33,34] Graphite oxide can be readily exfoliated in water to form single or a few layers of GO suspension, and the carboxylic functional groups on the edge cause these nanoplatelets to become negatively charged in an alkaline condition.[35] Based on this idea, we prepared a cationic waterborne polyurethane (CWPU) emulsion with positively charged latex particles dispersed in water. The particles with positive charges assemble onto the surface of the negatively charged GO nanoplatelets through electrostatic interactions in the process of that the GO suspensions was blended with the CWPU emulsion together. In result, the diffusion of PU macromolecules along the surface of the GO nanoplatelets prevents the aggregation of the GO nanoplatelets as drying. Finally, the PU/graphene nanocomposites were obtained through the chemical reduction of CWPU/GO in N, *N*-dimethylmethanamide (DMF) and dryness. After the chemical reduction of GO, electrostatic interaction between the positive charged urethane bond of CWPU and RGO nanoplatelets leads to the homogeneous dispersion of graphene in the PU matrix. The novelty of this work is the concept of preparation of PU/grapheme nanocomposite by using latex co-coagulation method for the first time. In addition, CWPU emulsion and GO suspension were used as starting materials. PU/graphene nanocomposites prepared in this method was endowed with enhanced thermal stability, electrical conductivity, and gas barrier property to a quietly high extend.

To confirm the electrostatic interaction between the positively charged polyurethane and the negatively charged graphene nanoplatelets, we prepared a negatively charged anionic waterborne polyurethane (AWPU) dispersion and the AWPU/RGO by following the same procedure.

EXPERIMENTAL

Materials

Natural flake graphite (99 wt % purity, average particle diameter of 20 μm) was obtained from Yingshida Graphite Co., Ltd. Hydrochloric acid, sodium nitrate, sulfuric acid (98%), potassium permanganate, hydrazine hydrate (80%), and hydrogen peroxide (30%) were purchased from Sinopharm Chemical Reagent Co., Ltd. (China) and used as received. DMF, triethylamine (TEA), and acetone were purchased from Sinopharm Chemical Reagent Co., Ltd. (China) and dried through four Å molecular sieves before use. Toluene-2, 4-diisocynate (TDI), *N*-methyldiethanolamine (MEDA), acetic acid, and 1, 4-butanediol (BG) were purchased from Aladdin Chemistry Co., Ltd. (China) and used as received. Poly(butylene adipate) (PBA) diol (1000 g/mol) was supplied by Qingdao Yutian Chemical Co., Ltd. and dried at 120°C under vacuum for 2 h. Dimethylol propionic acid (DMPA) was provided by Nippon Kasei Chemical Co., Ltd. and dried at 50°C for 48 h in a vacuum oven.

Preparation of GO Suspension

Graphite oxide was first fabricated from graphite by a modified Hummers method.[36] Concentrated H_2SO_4 (120 mL) was poured into a four-necked 500-mL flask and stirred in an ice bath until the temperature dropped to 0°C–5°C. Natural graphite (3 g) and $NaNO_3$ (5 g) were added and stirred uniformly. $KMnO_4$ (15 g) was gradually added with stirring and cooling to keep the temperature at 5–10°C. The solution was heated to 35°C and maintained at that temperature for 2 h. Then, distilled water (230 mL) was slowly added, and the temperature was kept at about 98°C. After 30 min, the reaction was terminated by the addition of 700 mL distilled water and a 30% H_2O_2 solution (15 mL). The mixture was filtered and washed with a 5% HCl aqueous solution to remove the sulphate ions and then centrifuged and washed with water. This process was repeated several times until the pH of the supernatant reached 7.0. The final product was subjected to dialysis to completely remove residual salts and acids. Finally, graphite oxide was redispersed in deionized water (DI) water by ultrasonication, and a dispersive GO suspension was obtained.

Preparation of CWPU Emulsion

The CWPU emulsion was prepared in a four-necked, round-bottom 500-mL flask equipped with a mechanical stirrer, condenser, and dropping funnel, under a dry nitrogen atmosphere in a constant temperature oil bath. First, PBA (0.05 mol), BG (0.017 mol), and TDI (0.106 mol) were placed into the flask and reacted at 75°C for 3 h. Then, MEDA (0.021 mol) dissolved in 20 mL acetone was added and the reaction was carried out for another 50 min at 45°C to produce the NCO-terminated polyurethane prepolymer. The number average molecular weight of the prepolymer calculated by feed was about 4000. Afterwards, acetic acid (0.02 mol) was fed into the reactor to neutralize the tertiary amine groups of the prepolymer. After 5 min, DI water (160 mL) was poured dropwise into the flask to

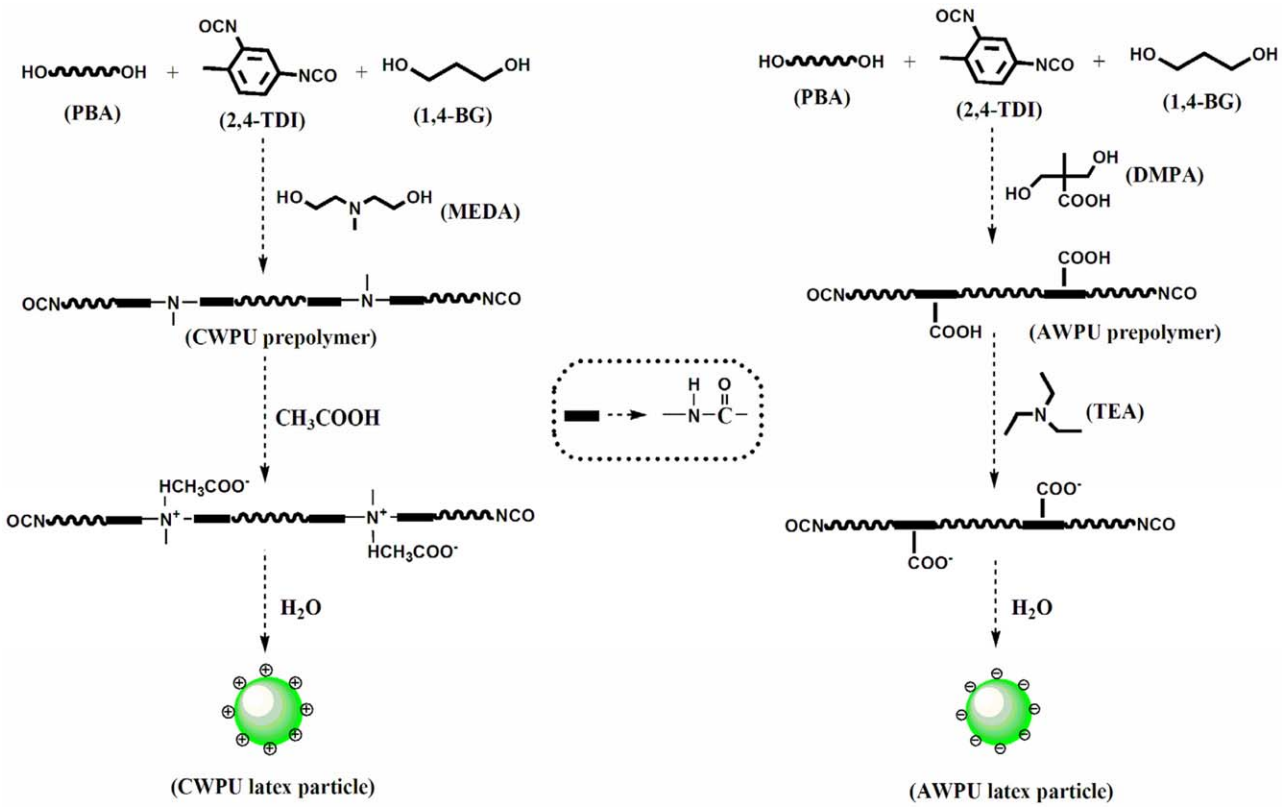

Scheme 1. Overall reaction scheme to prepare CWPU and AWPU emulsion. [Color figure can be viewed in the online issue, which is available at wileyonlinelibrary.com.]

obtain an aqueous emulsion. The emulsion was stirred at 45°C for the post-chain extension reaction completed within 3 h. The resulting product was a CWPU emulsion with a solid content of 30 wt %. The reaction scheme of preparation of CWPU emulsion is depicted in Scheme 1.

Preparation of AWPU Emulsion

The AWPU emulsion was prepared in a four-necked, round-bottom 500-mL flask equipped with a mechanical stirrer, condenser, and dropping funnel, under a dry nitrogen atmosphere in a constant temperature oil bath. First, PBA (0.05 mol), BG (0.017 mol), and TDI (0.106 mol) were placed into the flask and reacted at 75°C for 3.0 h. Then, DMPA (0.021 mol) dissolved in 20 mL DMF was added and the reaction was carried out for another 50 min at 70°C to produce the NCO-terminated polyurethane prepolymer. The number average molecular weight of the prepolymer calculated by feed was about 4000. Afterwards, TEA (0.02 mol) was added to neutralize the carboxyl unit of the prepolymer. After 5 min, deionized water (160 mL) was poured dropwise into the flask to obtain an aqueous emulsion. The emulsion was stirred at 45°C for the post-chain extension reaction completed within 3 h. The resulting product was an AWPU emulsion with a solid content of 30 wt %. The reaction scheme of preparation of AWPU emulsion is depicted in Scheme 1.

Preparation of CWPU/GO and AWPU/GO Nanocomposite

Six grams of the as-prepared synthetic CWPU emulsion was gradually added to the GO suspension (200 mL, 1.0 mg/mL). After being stirred for 1 h, the resultant settled mixture was filtered, washed several times with water, and then dried in a vacuum oven at 50°C for 24 h; the solid products were obtained as a CWPU/GO nanocomposite. The fabrication of the AWPU/GO nanocomposite followed the same procedure.

Preparation of CWPU/RGO and AWPU/RGO Nanocomposite

Four grams of the as-prepared solid CWPU/GO nanocomposite was added to 36 mL of DMF under ultrasonication to form a homogenous brown dispersion. After the addition of 0.1 mL hydrazine hydrate, the brown dispersion was transferred to a three-necked 100-mL flask for chemical reduction reaction at 80°C for 2 h. As the reduction proceeded, the brown dispersion of CWPU/GO turned black but remained homogenous without any precipitate. The as-prepared solid CWPU/RGO nanocomposite was added to DMF under ultrasonication to form a homogenous black dispersion. The dispersion was droplet cast onto a polytetrafluoroethylene (PTFE) mold plate (100 × 100 × 5 mm) and then dried in a vacuum oven at 60°C for 24 h to obtain a film of CWPU/RGO nanocomposite with a thickness of about 0.5 mm. The AWPU/RGO nanocomposite and film were prepared according to the same procedure.

Characterization Techniques

Fourier transform infrared spectrums (FT-IR) were conducted using a Nicolet 380 spectrometer at a resolution of 4 cm^{-1} with neat KBr as background. X-ray diffraction (XRD) analysis was carried out by using a Rigaku RAD-3C X-ray diffractometer (Japan) with Cu Kα radiation ($k = 0.154$ nm, 40 kV, 40 mA) as

the X-ray source. The sample was tested by scanning within the range of 5° to 60° at a step size of 0.02° and a scan speed of 0.1 s/length. The micromorphology of graphene and the nanocomposites were examined by transmission electron microscopy (TEM; JEOL 2100F, Japan) at an accelerating voltage of 200 kV. Solution samples were dropped onto a copper grid. After drying, it was used to take the TEM images of graphene. For the solid nanocomposites, the samples were cut to about 100-nm thickness at −160°C by using a Leica UC6 cryo-ultramicrotome (Germany) and then subjected to direct TEM observation. Atomic force microscopy (AFM) observation was done on the DI Multimode V (USA) in tapping mode at a scan rate of 1 Hz. The sample was prepared by spin-coating the DMF solution of RGO or CWPU/RGO onto freshly cleaved mica substrates at 1000 rpm. The scanning electron microscopy (SEM) images of the fractured surface of CWPU and nanocomposite were taken using a field emission scanning electron microscope (SU8020, Hitachi, Japan). Differential scanning calorimetry (DSC) was done with the DSC 823^e (Mettler Toledo, Switzerland) at a heating rate of 10°C/min. Thermogravimetric analysis (TGA) was done on a NETZSCH TG 209 thermogravimetric analyzer (Germany) to measure the thermal stability of the samples at a heating rate of 10°C/min from 35°C to 600°C. Zeta potential analysis was done with the Nanotrac Wave zeta potential analyzer (Microtrac Inc., USA). Electrical conductivity was measured by the standard four-point probe method (RTS-8; Guangzhou Four-Probe technology Co., Ltd. China). The nanocomposite films were cut into circular plates. Then, four electrode pins were pressed onto the paper surface with a spacing of 1 cm. Silver paste was placed at the contact points to eliminate contact resistance. For samples with low electrical conductivity, the test was done by using a megameter (1550C; Fluke Co., Ltd. USA) with 20-s charge time and 250 V of current stress. The films were cut into rectangular strips. An average value was obtained from three measurements for each sample. The resistance R can be obtained directly from the megameter; thus, the electrical conductivity σ can be calculated by using eq. (1):

$$\sigma = \frac{1}{\rho} = \frac{t}{RS} \quad (1)$$

where ρ is the electrical resistivity, t is the thickness of the sample between electrodes, and S is the cross-sectional area of the guarded cylinder electrode. The thermal diffusivity (α) of the nanocomposites was measured with the NETZSCH LFA 477 (Germany) at room temperature. The thermal conductivity (λ) was calculated by using eq. (2):

$$\lambda = \alpha \times \rho \times C_P \quad (2)$$

where α is the thermal diffusivity, C_P is the heat capacity, and ρ is the density of the nanocomposites. The oxygen transmission rate (OTR) was measured with the MOCON OX-TRAN model 2/21 (MOCON, Inc. USA). Samples were prepared by bar-coating the DMF solution of nanocomposites onto a poly (ethylene terephthalate) (PET, 25 μm thickness) substrate. DMF was evaporated by drying the coated samples in an oven at 80°C for 5 min. The samples were tested at 0% relative humidity (RH) at a temperature of 23°C. The film thickness was measured with the Filmetrics F20 (Filmetrics, Inc. USA).

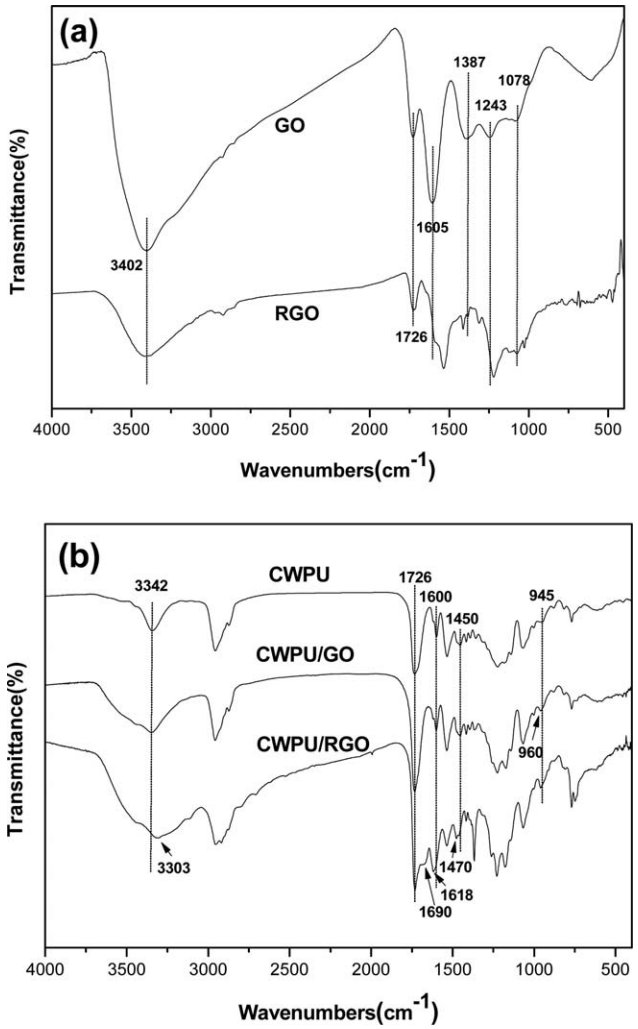

Figure 1. FT-IR spectra of GO, RGO (a); CWPU, CWPU/GO, and CWPU/RGO (b).

RESULTS AND DISCUSSION

FT-IR Analysis

The FT-IR spectra of GO, RGO, CWPU, CWPU/GO, and CWPU/RGO are shown in Figure 1. The FT-IR spectra of GO [Figure 1(a)] shows the corresponded characteristic peaks of C═O (1726 cm^{-1}), C—O—C (1078 cm^{-1}), —OH (1243 cm^{-1}), carboxyl C—O (1387 cm^{-1}), and aromatic C═C (1605 cm^{-1}). The broad absorption band at 3402 cm^{-1} is related to the —OH groups.[37–39] After the reduction, characteristic peaks of the GO disappeared except the —C═O at 1726 cm^{-1} in the spectrum of RGO, because the —COOH or —C═O groups at the edges of RGO sheets have not been removed completely. In addition, the peaks at 3416 cm^{-1} decreased significantly in contrast to GO, indicating that the vast majority of -OH groups or water has been removed.

Figure 1(b) shows the FT-IR spectra of CWPU, CWPU/GO, and CWPU/RGO nanocomposites. The spectra of CWPU shows

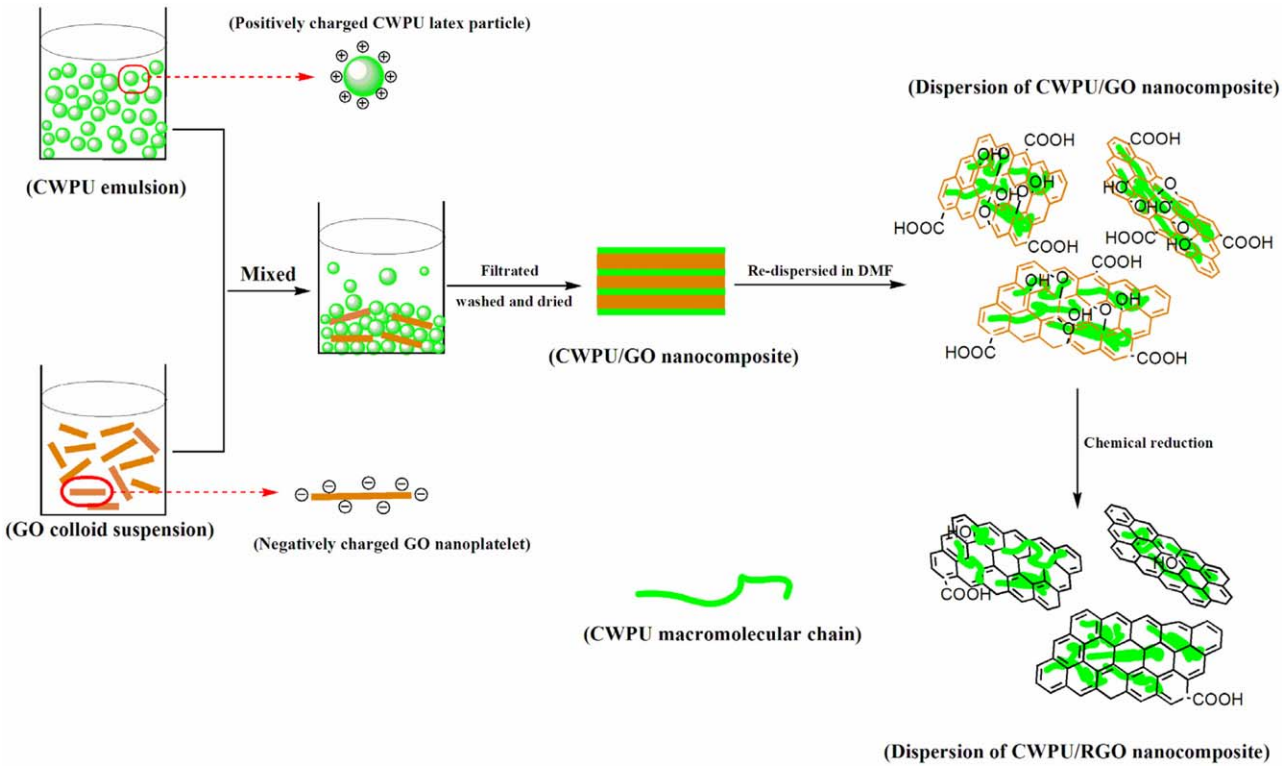

Figure 2. Schematic illustration of the fabrication of CWPU/RGO. [Color figure can be viewed in the online issue, which is available at wileyonlinelibrary.com.]

characteristic bands of urethane N-H at 3342 cm^{-1} and C═O stretching of the urethane linkage at 1726 cm^{-1}. The aromatic C═C band of benzene ring from TDI was observed around 1600 cm^{-1} and 1450 cm^{-1}. The band at 1533 cm^{-1} was because of the C—N stretching. The peak at 945 cm^{-1} confirms the presence of aliphatic quaternary ammonium salts. As for CWPU/RGO, the peak position of N-H generally moves from 3342 to 3303 cm^{-1}. In addition, the presence of band at 1690 cm^{-1} can be attributed to the hydrogen bonded C═O (the free C═O stretching peaks at 1726 cm^{-1}), which indicates the hydrogen interactions between urethane bond and RGO nanoplatelets. The peaks at 1600 and 1450 cm^{-1} moved to 1618 and 1470 cm^{-1}, respectively, suggesting that the aromatic C═C band in hard segments interacted with RGO nanoplatelets through π-π interactions. However, these changes have not been detected in CWPU/GO, indicating the absence of hydrogen or π-π interactions between CWPU and GO nanoplatelets. The peak of aliphatic quaternary ammonium at 945 cm^{-1} for CWPU moved to 960 cm^{-1} for CWPU/GO and CWPU/RGO, indicating the electrostatic interactions between CWPU and graphene nanoplatelets. The FT-IR analysis confirmed that GO has been successfully reduced to RGO, and RGO nanoplatelets was attached to CWPU through hydrogen, π-π, and electrostatic interactions.

Dispersion of the CWPU/RGO

The fabrication of the CWPU/RGO nanocomposite was done in three steps, as shown in Figure 2. First, the negatively charged GO aqueous suspension was mixed with the positively charged CWPU emulsion. After that, the sediment of the mixture was filtrated, washed, and dried to prepare solid CWPU/GO nanocomposite. Second, a homogenous DMF solution of CWPU/GO was obtained by re-dispersing the solid CWPU/GO nanocomposite in DFM. Finally, chemical reduction was done with hydrazine hydrate as the reducing agent to convert the CWPU/GO to CWPU/RGO. Optical observations were carried out to illustrate the fabrication process, as shown in Figure 3. The GO aqueous suspension and CWPU emulsion are shown to be very stable in Figure 3(a,b). Zeta potentials presented in Table I confirm that such aqueous suspensions are ideal for stabilizing conventional colloidal particles.[40] The mixture was quickly precipitated after the GO aqueous suspension and CWPU emulsion were combined, as shown in Figure 3(c). The solid CWPU/GO nanocomposite could be easily re-dispersed in DMF to form a homogenous and stable yellowish-brown DMF solution [Figure 3(d)]. After reduction, the yellowish-brown color of the CWPU/GO solution changed into black, suggesting the successful reduction of GO in the presence of CWPU [Figure 3(e)]. The black dispersion was stable, and no obvious precipitates were observed after storage for several months. The zeta potential was −43.3 mV, which also confirmed the stability of the DMF solution of CWPU/RGO.[41] To illustrate the electrostatic interaction between the CWPU and graphene nanoplatelets (GO or RGO), a kind of negatively charged WPU emulsion (AWPU) was prepared and used to fabricate AWPU/GO and AWPU/RGO according to the same process applied for CWPU. As shown in Figure 3(g), the mixture of the AWPU emulsion with the GO suspension and DMF solution of AWPU/GO was stable. However, the DMF solution of AWPU/RGO was precipitated

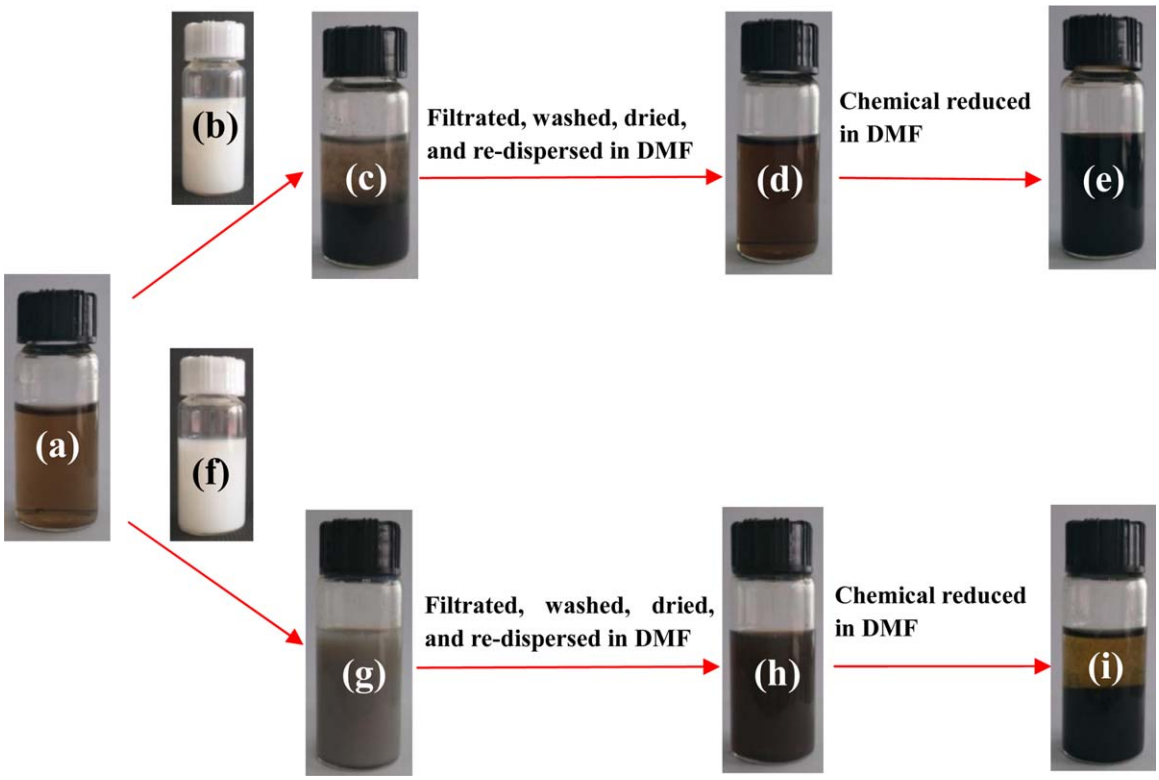

Figure 3. Photograph of GO aqueous suspension (a), CWPU emulsion (b), complex of CWPU emulsion and GO suspension (c), DMF solution of CWPU/GO (d), DMF solution of CWPU/RGO (e), AWPU emulsion (f), complex of AWPU emulsion and GO suspension (g), DMF solution of AWPU/GO (h), and DMF solution of AWPU/RGO (i). [Color figure can be viewed in the online issue, which is available at wileyonlinelibrary.com.]

completely after several hours of storage. Fourier transform infrared spectroscopy (FTIR) investigation confirmed that the substance in the supernatant was AWPU and the sediment was RGO (as shown in Supporting Information Fig. S1). This finding indicates that, unlike the positively charged CWPU, the negatively charged AWPU cannot disperse and stabilize the RGO nanoplatelets. In addition, it is worth noting that a stronger sonication power and a longer time are required to redisperse the solid mixture of AWPU/GO compared with CWPU/GO. Nevertheless, a small quantity of solid substance cannot disperse, which might result in the re-aggregated GO nanoplatelets formed in the drying process. Above results confirm that CWPU interacted with the RGO (or GO) nanoplatelets through electrostatic interaction and the inclusion of CWPU within the interlayer spaces of RGO (or GO) might have separated the nanoplatelets, preventing nanoplatelets from aggregating.

Table I. Zeta Potentials of Different Types of Samples

Samples	Zeta potential (mV)	Solvent	Serial number in Figure 3
GO	−46.8	Water	a
CWPU	47.7	Water	b
CWPU/GO	–	Water	c
CWPU/GO	57.9	DMF	d
CWPU/RGO	−43.3	DMF	e
AWPU	−51.2	Water	f
AWPU/GO	−39.6	Water	g
AWPU/RGO	−36.8	DMF	h
AWPU/RGO	–	DMF	i

Morphology of the CWPU-Coated RGO

TEM was used to investigate the morphology and exfoliation of the CWPU-coated RGO nanoplatelets, as shown in Figure 4. Several layers of platelets could be observed in the TEM image of RGO [Figure 4(a)], indicating the aggregation of RGO nanoplatelets. In contrast, the CWPU/RGO consisted of thin transparent layers and showed the transparent morphology of a well-exfoliated graphene sheet [Figure 4(b)]. Note that there is no apparent coiled graphene, which is attributed to the adsorbed CWPU chains. The morphology analysis suggests that RGO nanoplatelets coated with CWPU are well dispersed and exfoliated in DMF. In addition, TEM image of GO aqueous suspension, CWPU emulsion, and CWPU/GO complex are presented in Figure 4(c-e). As can be seen from Figure 4(e), the dyed CWPU latex particles (dark part) burst and spread out on the surfaces of GO nanoplatelets (transparent part) irregularly, suggesting the strong attractions between the CWPU and GO.

To confirm the RGO nanoplatelets were coated with CWPU, we measured the thickness of the CWPU/RGO by AFM observation. Figure 5 shows the tapping-mode AFM images of RGO and CWPU/RGO dispersed in DMF. The samples were prepared by depositing the corresponding dispersions on new cleaved mica surfaces and then drying them in air. From the cross-

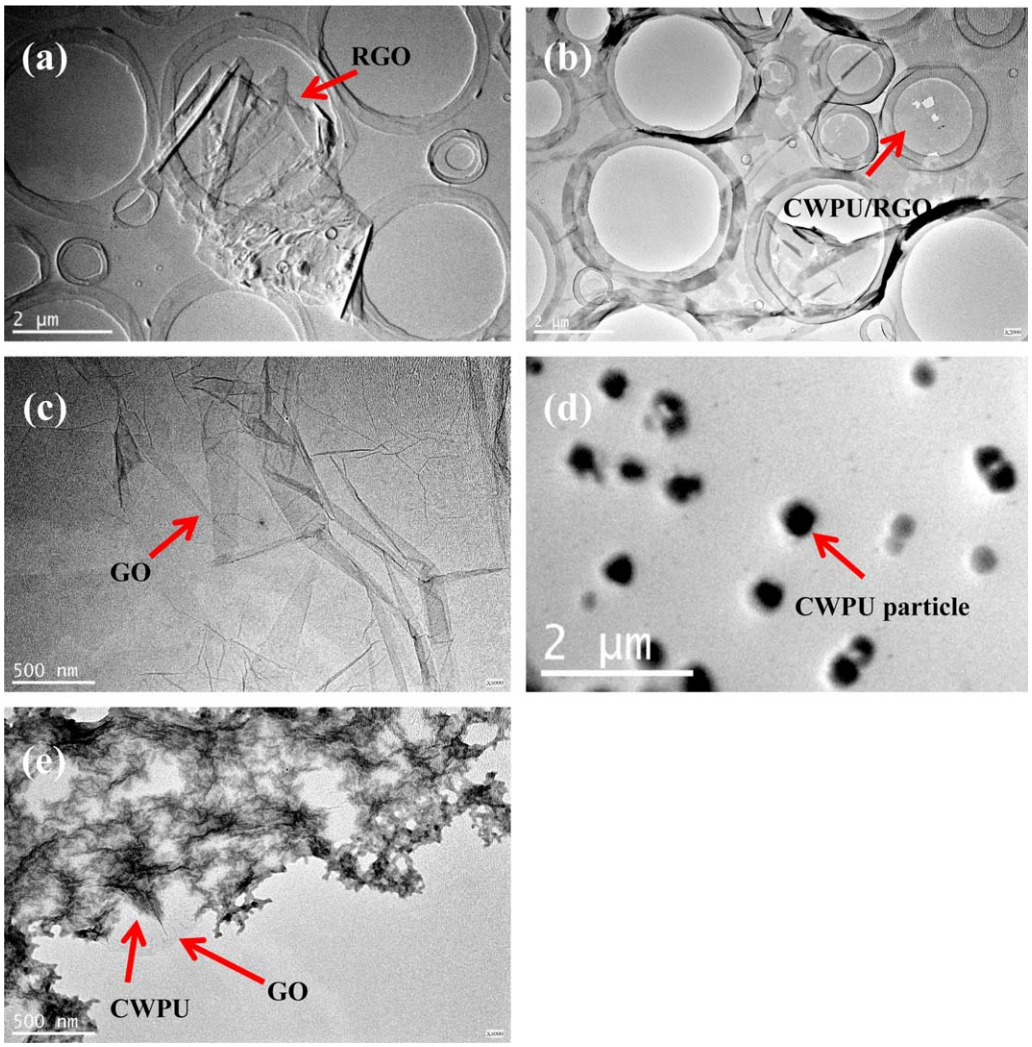

Figure 4. TEM image of RGO (a), CWPU/RGO (b), GO (c), CWPU emulsion (d), and CWPU/GO complex (e). [Color figure can be viewed in the online issue, which is available at wileyonlinelibrary.com.]

section analysis, we determined that the RGO nanoplatelets had a height of around 1.116 nm [Figure 5(a)]. The thickness of the CWPU/RGO nanoplatelet was about 3.208 nm, which was much larger than that of the RGO. This could be attributed to the CWPU macromolecules, which covered the graphene nanoplatelets.[42] The increased thickness of the CWPU/RGO sheet also implies that CWPU macromolecules uniformly coated the surface of the RGO nanoplatelets and that strong interactions exist between the two.

Dispersibility of RGO in CWPU Matrix

The performance of nanocomposites depends strongly on the dispersion state of the nanofillers and their interaction with the polymer matrices.[43] Herein, the dispersibility of the RGO nanoplatelets in the PU matrix was studied by XRD, TEM, FESEM, and Raman analysis.

The XRD spectrum of pristine graphite displayed a sharp and narrow peak at 2θ=26.5°, as shown in Figure 6(a). By using the Bragg equation ($n\lambda = 2d \sin \theta$), the interlayer distance of graphene nanoplatelets was calculated as 0.34 nm. In the case of GO, this peak disappeared and a new diffraction peak appeared at approximately 11.3°, suggesting that the interlayer spacing increased to 0.78 nm. The large interlayer distance is attributed to the formation of hydroxyl, epoxy, and carboxyl groups, which increases the interlayer spacing of GO. This result is in accordance with previous reports[43] and shows that well-exfoliated GO sheets in water tend to re-aggregate during the drying process. After chemical reduction, the peak of GO at 11.3° disappeared, but a broad and weak peak appeared at around 25.0° (d-spacing = 0.36 nm), indicating that the restacking and aggregation of RGO nanoplatelets occurred during the chemical reduction of GO.[44]

Figure 6(b) shows the XRD spectra of the solid CWPU/GO and CWPU/RGO nanocomposites. The spectrum of CWPU/GO shows no characteristic diffraction peak at around 11.3°, indicating that the CWPU prevented the GO nanoplatelets from aggregating. Similarly, the broad peak at 25.0° in the XRD spectrum of the CWPU/RGO nanocomposite is not present, which suggests that CWPU efficiently coated the surface of the RGO nanoplatelets, preventing their aggregation. Peaks at around

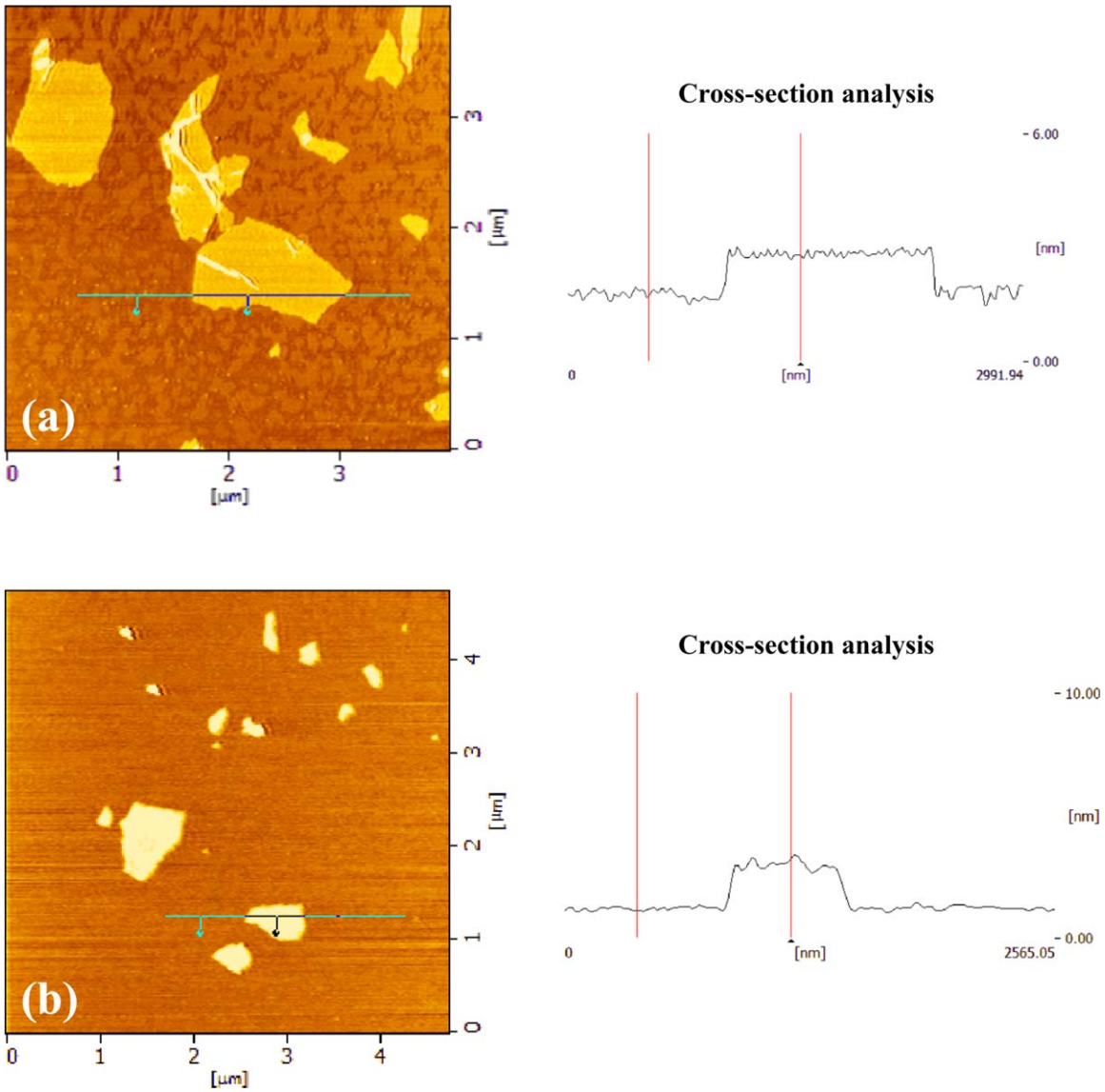

Figure 5. AFM image and cross-section analysis of RGO (a) and CWPU/RGO (b). [Color figure can be viewed in the online issue, which is available at wileyonlinelibrary.com.]

21.0°, 22.0°, and 24.0° are originating from CWPU. Thus, the RGO nanoplatelets were considered to be well dispersed and exfoliated in the CWPU matrix. The result is similar to CWPU/GO because the RGO nanoplatelets are also negatively charged.[45] It is worth noting that the characteristic peaks of CWPU are not observed in the XRD spectrum of the CWPU/GO nanocomposite, probably because oxygen groups on the surface of the GO nanoplatelets hindered the crystallization of CWPU. In the case of AWPU, as presented in Figure 6(c), the XRD spectrum of AWPU/GO shows a peak at 8.3°. Moreover, the broad peak at 25.0° in the XRD spectrum of the AWPU/RGO nanocomposite is present. These results indicate that negatively charged AWPU cannot prevent the reaggregation of RGO and GO nanoplatelets like positively charged CWPU.

The dispersion status of graphene sheets in the polymer matrix can be observed by direct TEM and FESEM. Figure 7(a) shows the TEM image of the CWPU/RGO nanocomposite. The RGO nanoplatelets were finely dispersed throughout the CWPU matrix in a wrinkled or paper-like structure, and most of the nanoplatelets mainly had an intercalated morphology, except for some areas that contained a few exfoliated RGO nanoplatelets. As for AWPU/RGO [Figure 7(b)], the TEM image suggested that the RGO nanoplatelets re-aggregated in the AWPU matrix obviously. Figure 7(c–f) shows the FESEM images of neat CWPU, CWPU/RGO nanocomposite, and AWPU/RGO. The neat CWPU matrix [Figure 7(c)] shows a flat and smooth fractured surface. In contrast, the incorporation of RGO nanoplatelets resulted in the formation of many irregular protuberances evenly distributed on the fracture surface, as shown in Figure 7(d). In addition, the RGO protrusions perfectly coated with CWPU can be clearly seen from the higher magnification image [Figure 7(e)], indicating the strong polymer and RGO

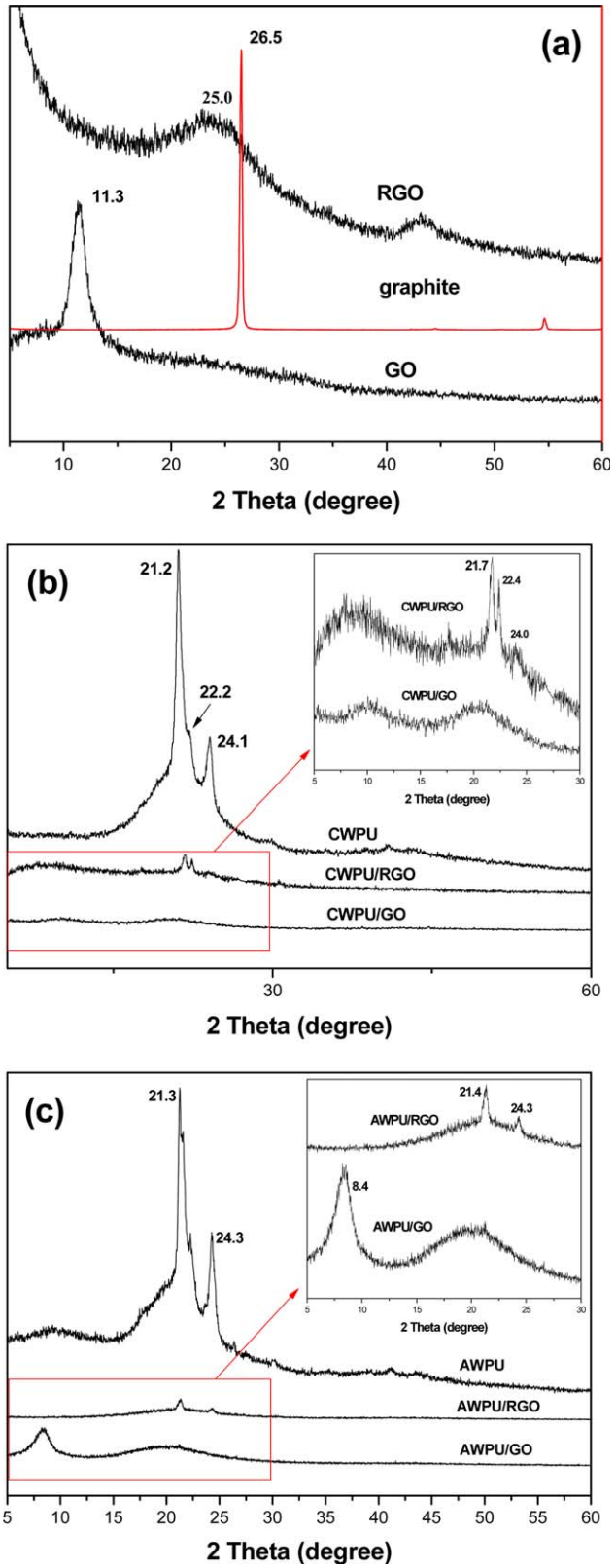

Figure 6. XRD spectra of graphite, GO, and RGO (a); CWPU, CWPU/GO, and CWPU/RGO (b); AWPU, AWPU/GO, and AWPU/RGO (c). [Color figure can be viewed in the online issue, which is available at wileyonlinelibrary.com.]

interaction. However, in the case of AWPU, the re-aggregation RGO could be obviously observed suggesting poor dispersibility of the RGO nanoplatelets with AWPU [Figure 7(f)]. The XRD, TEM, and FESEM results suggest that electrostatic interactions are favorable for the homogeneous dispersion of RGO nanoplatelets in the CWPU matrix and the strong interfacial interaction between them.

The Raman spectrum was also investigated to confirm the dispersion status of the RGO nanoplatelets in the CWPU matrix. The D mode is a combination of the symmetry optical phonon A_{1g} at point K of the Brillouin zone due to the breathing vibration of aromatic rings, whereas the G band corresponds to the first-order scattering of the mode E_{2g}.[46] Figure 8 shows the Raman spectra of RGO and the CWPU/RGO nanocomposite. The G band of RGO observed at 1598.5 cm^{-1} is markedly broadened and shifted to 1610.7 cm^{-1} in the CWPU/RGO nanocomposite, indicating that the RGO nanoplatelets were well dispersed and exfoliated in the CWPU matrix.[47] This is in good agreement with the XRD, TEM, and FESEM results.

It is worthwhile to note that although AWPU (containing benzene ring and urethane bond) can form hydrogen and π–π interactions with RGO nanoplatelets like CWPU, which was confirmed by FT-IR analysis. However, RGO nanoplatelet has much better dispersion ability in CWPU than in AWPU. This result confirms that the electrostatic interaction is the main factor which leading to the homogeneous dispersion of graphene in the PU matrix and the strong interfacial interaction between them.

Thermal Analysis of CWPU/RGO Nanocomposite

CWPU is a semicrystalline polymer, as confirmed by the XRD spectra. The DSC thermogram of the CWPU resin shows the melting endothermic peaks at 29.8°C and 38.7°C, as shown in Figure 9. In the case of the CWPU/RGO nanocomposite, the melting endothermic peaks shift to 32.3°C and 39.2°C, respectively. This result indicates that the crystallization temperature of CWPU moved to a higher temperature due to the incorporation of RGO nanoplatelets. The reason for this may be that the incorporated graphene fillers acted as barriers that prevented the propagation of heat from the extraneous surroundings into the polymeric matrices. A new melting endothermic peak was observed at 68.8°C, suggesting that graphene acted as a nucleus from which a new type of crystallization morphology of CWPU was induced. The DSC results indicate that the molecular-level dispersion of RGO nanoplatelets in the CWPU matrix not only effectively improved the degree of crystallinity of the PU material but also raised the temperature of crystalline melting.

Figure 10 presents the results of the TGA of GO, RGO, CWPU, and the CWPU/RGO nanocomposite. The TGA curves show that the degradation temperature of CWPU shifted toward higher temperatures after the incorporation of RGO nanoplatelets, indicating the enhanced thermal stability of the nanocomposite. This result is in good agreement with our DSC results. Moreover, based on the TGA results, we could calculate the weight fraction of RGO in the CWPU/RGO nanocomposite. The weight ratios of the residues obtained for GO, RGO, CWPU, and CWPU/RGO were approximately 62.9%, 88.1%,

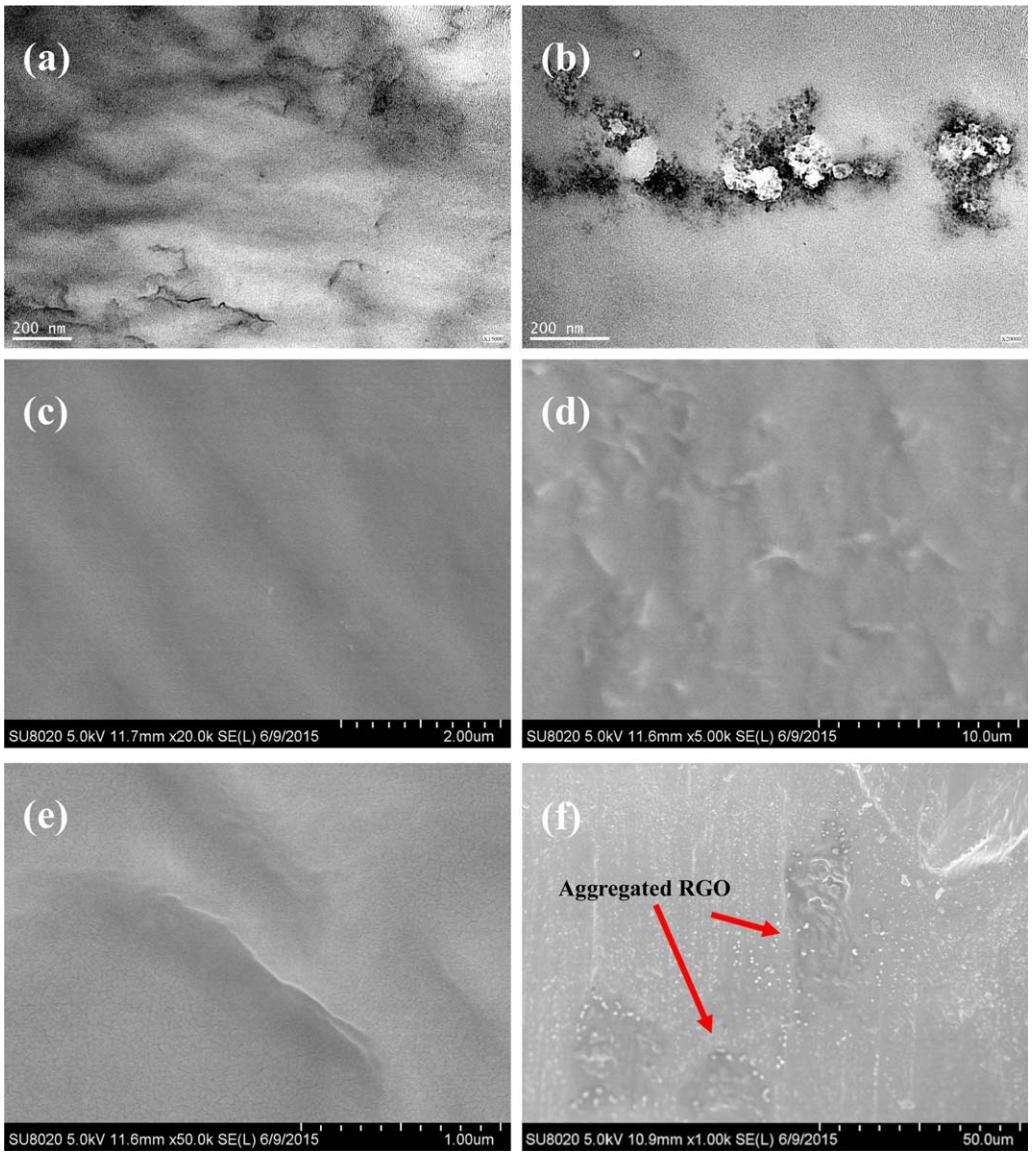

Figure 7. TEM image of CWPU/RGO (a) and AWPU/RGO (b); FESEM image of CWPU (c), CWPU/RGO (d,e), and AWPU/RGO (f). [Color figure can be viewed in the online issue, which is available at wileyonlinelibrary.com.]

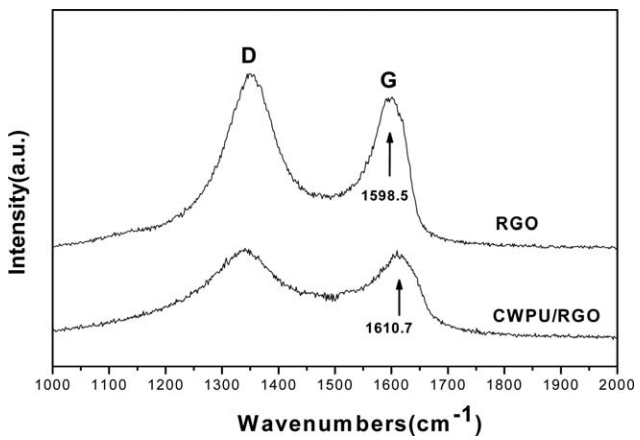

Figure 8. Raman spectra of RGO and CWPU/RGO.

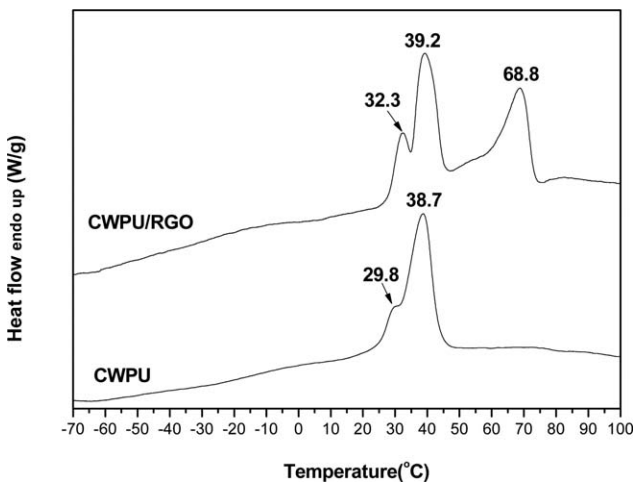

Figure 9. DSC thermograms of CWPU and CWPU/RGO.

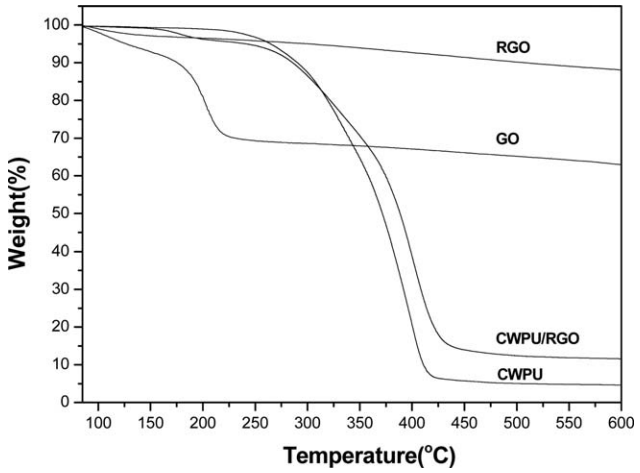

Figure 10. TGA curves of GO, RGO, CWPU, and CWPU/RGO.

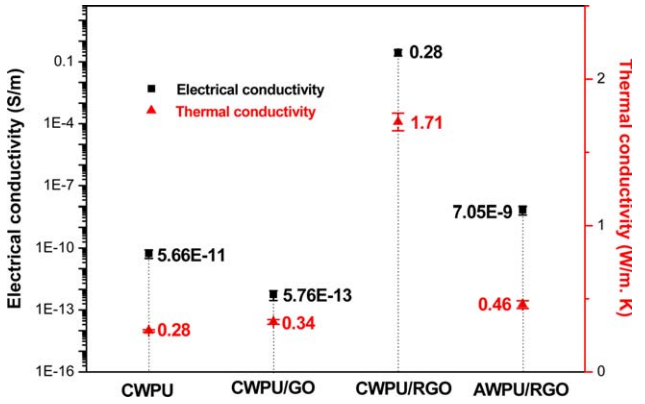

Figure 11. Electrical and thermal conductivity of different types of samples. [Color figure can be viewed in the online issue, which is available at wileyonlinelibrary.com.]

4.5%, and 12.2%, respectively, at 600°C. According to a previous report,[48] the total weight of a CWPU/RGO nanocomposite is obtained as $m_t = m_p + m_g$, where m_p is the weight of the CWPU adsorbed on the graphene nanoplatelets, and m_g is the weight of the RGO in the nanocomposite. Therefore, we calculated that the weight fraction of RGO in the CWPU/RGO nanocomposite was about 9.2%, whereas the weight fraction of GO in the CWPU/GO nanocomposite was 10.0%. The decreased weight fraction can be attributed to the removal of oxygen groups in the GO nanoplatelets.

Electrical and Thermal Conductivity of CWPU/RGO Nanocomposite

Pristine graphene shows excellent thermal and electrical conductivity. Conductive polymer nanocomposites were obtained by the incorporation of graphene sheets into different polymer resins. The thermal conductivity of a nanocomposite is well known to be affected by the dispersion of the nanofiller within the matrix and the thermal resistance of the interface between the nanofillers and the polymeric matrix.[49] The thermal conductivity of CWPU/RGO was investigated, and the results are shown in Figure 11. The CWPU/GO nanocomposite showed a thermal conductivity of 0.34 W m^{-1} K^{-1}, which is close to that of pure CWPU (0.28 W m^{-1} K^{-1}). In comparison, the thermal conductivity of the CWPU/RGO nanocomposite was 1.71 W m^{-1} K^{-1} which was much higher than CWPU/GO. This is because the destroyed structure of the GO sheet was restored by chemical reduction. In the case of AWPU, the thermal conductivity of the AWPU/RGO nanocomposite was 0.46 W m^{-1} K^{-1}, which is significantly less than that of CWPU/RGO. This result suggests that the good dispersion and exfoliation of RGO in the CWPU matrix effectively enhanced the thermal conductivity of the nanocomposite. In addition, the electrostatic interactions between the RGO nanoplatelets and CWPU resin reduced the interfacial thermal resistance effectively and improved the phonon transportation in the nanocomposite.

The electrical conductivity of different configurations was also tested, and the results showed in Figure 11. The electrical conductivity values of CWPU and CWPU/GO were 5.66 E-11 S m^{-1} and 5.76 E-13 S m^{-1}, respectively, indicating their insulating behavior. However, the CWPU/RGO nanocomposite showed an electrical conductivity of 0.28 S m^{-1}. This remarkable enhancement in electrical conductivity indicates that the GO nanoplatelets had been highly reduced in the CWPU/RGO nanocomposite, and conductive networks of RGO had formed. The AWPU/RGO nanocomposite showed a conductivity of 7.05E-9 S m^{-1}, which is much less than that of the CWPU/RGO nanocomposite. This result indicates that the well-dispersed RGO nanoplatelets with high aspect ratios in the CWPU matrix facilitated the construction of conductive networks. Moreover, because of the favorable interfacial interactions arising from electrostatic attraction, the RGO nanoplatelets showed good compatibility with the CWPU matrix. Such homogeneous dispersion contributed to the construction of an electrical conductive pathway.

Oxygen Barrier Properties of CWPU/RGO Nanocomposite

The oxygen transmission rate (OTR) of the CWPU/RGO nanocomposite-coated PET films was measured, as shown in Figure 12. The samples were prepared by coating DMF solutions of different configurations onto the PET substrate and then removing the DMF by heating. The OTR shown in Figure 12(a) indicated that CWPU has poor O_2 barrier property because CWPU-coated PET film has a similar OTR to that of neat PET film. CWPU/GO-coated PET films showed a remarkable enhancement in OTR compared with neat PET film. For example, the OTR of CWPU-coated PET film was 115.3 cm^3 m^{-2} day^{-1}, whereas that of CWPU/GO was 22.3 cm^3 m^{-2} day^{-1}. This result indicates the high gas barrier property of CWPU/GO; the impermeable GO in the CWPU matrix increases the path tortuosity and decreases the O_2 permeability, leading to a dramatic decrease in O_2 permeability through the nanocomposite films. Furthermore, the OTR of the CWPU/RGO-coated PET film decreased to 8.9 cm^3 m^{-2} day^{-1}, indicating its better gas barrier property compared with CWPU/GO. The extraordinary gas barrier performance of CWPU/RGO is attributed, first, to the low-defect RGO structure, which produces a highly impermeable material with increased barrier efficiency; this is the main difference between RGO and GO-related materials that have more defects. Second, RGO was well dispersed in the CWPU matrix. Herein, this uniform distribution of RGO created a very tortuous path for diffusion. However, in the case of AWPU/RGO-coated PET film, the OTR was 88.4 cm^3 m^{-2} day^{-1}, much higher than that of the CWPU/RGO

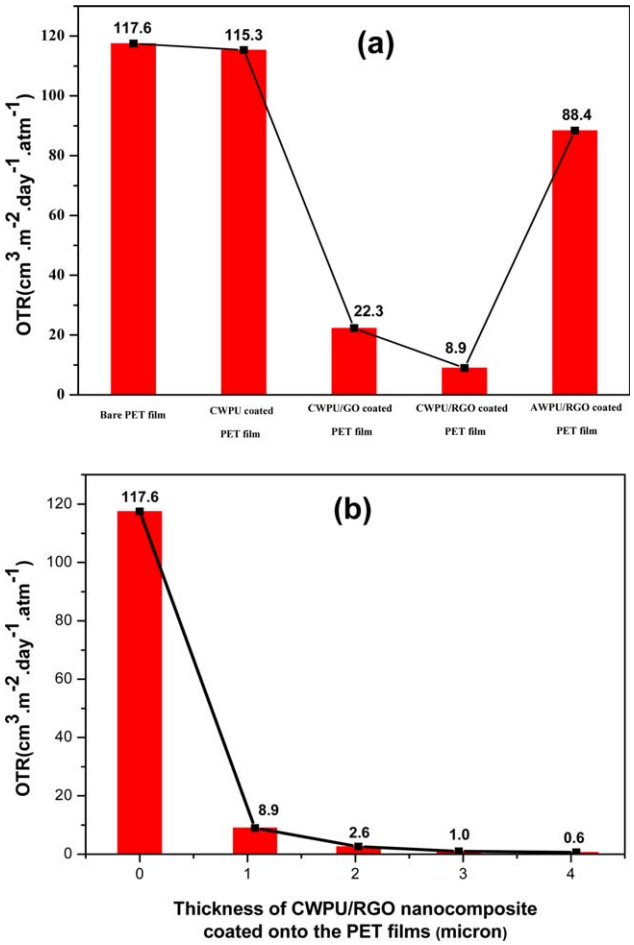

Figure 12. OTR for PET films coated with different types of samples (a) and the effect of the thicknesses of CWPU/RGO nanocomposite on the OTR (b). [Color figure can be viewed in the online issue, which is available at wileyonlinelibrary.com.]

nanocomposite, indicating the poor dispersion of RGO in AWPU. This result suggests that the improvement in gas barrier property is attributed to the decrease in the available area for diffusion and the creation of a tortuous pathway for permeating molecules.[50] To investigate the relationship between the thicknesses of the nanocomposites coated on the PET film and their oxygen barrier properties, we prepared samples of PET films with CWPU/RGO nanocomposite coatings of increased thicknesses of 2.03, 2.96, and 4.05 μm, respectively. The coating thickness was controlled by adjusting the solid content of the DMF solution of the CWPU/RGO nanocomposite. Figure 12(b) shows the effect of the CWPU/RGO coating thicknesses on the OTR. The OTR of the films decreased to 2.6, 1.0, and 0.6 $cm^3\ m^{-2}\ day^{-1}$, respectively, indicating that the OTR decreases with increasing thickness of CWPU/RGO nanocomposite coating. The enhanced oxygen barrier performances were attributed to the impermeability of RGO nanoplatelets, their complete exfoliation and random dispersion, and the strong interfacial adhesion between the RGO nanoplatelets and CWPU matrix.

CONCLUSION

This study presented a novel method of preparing a graphene/PU nanocomposite by using the latex co-coagulation technique. The synthesis was carried out by first mixing a negatively charged GO aqueous suspension with a positively charged CWPU emulsion, followed by chemical reduction of the CWPU/GO mixture in a DMF solution. The XRD, TEM, FESEM, and Raman analysis results showed that RGO nanoplatelets were well dispersed and exfoliated in the solid CWPU/RGO nanocomposite because of the electrostatic interactions between the graphene and polymer matrix. The fabricated CWPU/RGO nanocomposite showed a significant improvement in terms of its electrical and thermal conductivity, which improved by more than nine orders of magnitude and by 6.1 times, respectively, compared with the pure CWPU sample. Furthermore, with a coating thickness of ~4μm, the OTR of the CWPU/RGO nanocomposite-coated PET film can reach up to 0.6 $cm^3\ m^{-2}\ day^{-1}$. These improvements in the electrical and thermal conductivity and gas barrier properties of the CWPU/RGO nanocomposite could be attributed to the good dispersion of the high-aspect-ratio RGO nanoplatelets in the matrix and the electrostatic interactions between the RGO nanoplatelets and CWPU matrix. The method presented herein provides a promising approach to the fabrication of graphene-based polymeric nanocomposite coatings.

ACKNOWLEDGMENTS

This work was financially supported by the National Natural Science Foundation of China (grant no. 51273054) and the Natural Science Foundation of the Anhui Higher Education Institutions of China (grant no. KJ2015A205).

REFERENCES

1. Yadav, S. K.; Mahapatra, S. S.; Cho, J. W. *Polymer* **2012**, *53*, 2023.
2. Deka, H.; Karak, N.; Kalita, R. D.; Buragohain, A. K. *Carbon* **2010**, *48*, 2013.
3. Cai, D. Y.; Song, M. *Macromol. Chem. Phys.* **2007**, *208*, 1183.
4. Saha, C.; Chaki, T. K.; Singha, N. K. *J. Appl. Polym. Sci.* **2013**, *5*, 3328.
5. Lee, C. G.; Wei, X. D.; Kysar, J. W.; Hone, J. *Science* **2008**, *321*, 385.
6. Lee, G. H.; Cooper, R. C.; An, S. J.; Lee, S.; van der Zande, A.; Petrone, N.; Hammerberg, A. G.; Lee, C.; Crawford, B.; Oliver, W.; Kysar, J. W.; Hone, J. *Science* **2013**, *340*, 1073.
7. Du, X.; Skachko, I.; Barker, A.; Andrei, E. Y. *Nat. Nanotechnol.* **2008**, *3*, 491.
8. Balandin, A. A.; Ghosh, S.; Bao, W. Z.; Calizo, I.; Teweldebrhan, D.; Miao, F.; Lau, C. N. *Nano Lett.* **2008**, *8*, 902.
9. Stoller, M. D.; Park, S.; Zhu, Y. W.; An, J. H.; Ruoff, R. S. *Nano Lett.* **2008**, *8*, 3498.
10. Bunch, J. S.; Verbridge, S. S.; Alden, J. S.; Zande, A. M.; Parpia, J. M.; Craighead, H. G.; McEuen, P. L. *Nano Lett.* **2008**, *8*, 2458.
11. Tien, H. W.; Huang, Y. L.; Yang, S. Y.; Hsiao, S. T.; Wang, J. Y.; Ma, C. C. M. *J. Mater. Chem.* **2011**, *21*, 14876.

12. Hsiao, S. T.; Ma, C. C. M.; Liao, W. H.; Wang, Y. S.; Li, S. M.; Huang, Y. C.; Yang, R. B.; Liang, W. F. *ACS Appl. Mater. Inter.* **2014**, *6*, 10667.
13. Yousefi, N.; Gudarzi, M. M.; Zheng, Q. B.; Lin, X. Y.; Shen, X.; Jia, J. J.; Sharif, F.; Kim, J. K. *Compos. Part A* **2013**, *49*, 42.
14. Xiang, C. S.; Cox, P. J.; Kukovecz, A.; Genorio, B.; Hashim, D. P.; Yan, Z.; Peng, Z. W.; Hwang, C. C.; Ruan, G. D.; Samuel, E. L. G.; Sudeep, P. M.; Konya, Z.; Vajtai, R.; Ajayan, P. M.; Tour, J. M. *ACS Nano* **2013**, *7*, 10380.
15. Lin, S. C.; Buehler, M. *J. Nanotechnology.* **2013**, *24*, 165702.
16. Shen, J. F.; Hu, Y. Z.; Li, C.; Qin, C.; Ye, M. G. *Small* **2009**, *1*, 82.
17. Zhang, C. Z.; Hao, R.; Liao, H. B.; Hou, Y. L. *Nano Energy* **2013**, *2*, 88.
18. Shan, C.; Yang, H.; Han, D.; Zhang, Q.; Ivaska, A.; Niu, L. *Langmuir* **2009**, *25*, 12030.
19. Hao, R.; Qian, W.; Zhang, L. H.; Hou, Y. L. *Chem. Commun.* **2008**, *48*, 6576.
20. Wajid, A. S.; Das, S.; Irin, F.; Ahmed, H. S. T.; Shelburne, J. L.; Parviz, D.; Fullerton, R. J.; Jankowski, A. F.; Hedden, R. C.; Green, M. J. *Carbon* **2012**, *50*, 526.
21. Wang, G.; Hu, Y.; Song, L.; Yang, H.; Xing, W.; Lu, H. *J. Mater. Chem.* **2011**, *21*, 4222.
22. Li, Y. Q.; Pan, D. Y.; Chen, S. B.; Wang, Q. H.; Pan, G. Q.; Wang, T. G. *Mater. Design.* **2013**, *47*, 850.
23. Kumar, M.; Chung, J. S.; Kong, B. S.; Kim, E. J.; Hur, S. H. *Mater. Lett.* **2013**, *106*, 319.
24. Lee, Y. R.; Raghu, A. V.; Jeong, H. M.; Kim, B. K. *Macromol. Chem. Phys.* **2009**, *15*, 1247.
25. Ding, J. N.; Fan, Y.; Zhao, C. X.; Liu, Y. B.; Yu, C. T.; Yuan, N. Y. *J. Compos. Mater.* **2012**, *46*, 747.
26. Jaber, N. G.; Hossein, A.; Mohsen, M. G. *J. Mater. Sci.* **2014**, *49*, 243.
27. Kim, H.; Miura, Y.; Macosko, C. W. *Chem. Mater.* **2010**, *22*, 3441.
28. Liao, K. H.; Park, Y. T.; Abdala, A.; Macosko, C. *Polymer* **2013**, *54*, 4555.
29. Khan, U.; May, P.; O'Neill, A.; Coleman, J. N. *Carbon* **2010**, *48*, 4035.
30. Nguyen, D. A.; Lee, Y. R.; Raghu, A. V.; Jeong, H. M.; Shi, C. M.; Kim, B. K. *Polym. Int.* **2009**, *58*, 412.
31. Król, P.; Król, B.; Pielichowska, K.; Špírková, M. *Colloid Polym. Sci.* **2015**, *293*, 421.
32. Król, P.; Król, B.; Zenker, M.; Subocz, J. *Colloid Polym. Sci.* **2015**, *293*, 2941.
33. Cai, D.; Song, M. *Carbon* **2008**, *46*, 2107.
34. He, S.; Wang, Y.; Feng, Y.; Liu, Q.; Zhang, L. *Nanotechnology* **2010**, *21*, 115601.
35. Si, Y. C.; Samulski, E. T. *Nano Lett.* **2008**, *6*, 1679.
36. Hummers, W. S.; Offeman, R. E. *J. Am. Chem. Soc.* **1958**, *6*, 1339.
37. Stankovich, S.; Piner, R. D.; Nguyen, S. T.; Ruoff, R. S. *Carbon* **2006**, *44*, 3342.
38. Paredes, J. I.; Villar-Rodil, S.; Martinez-Alonso, A.; Tascon, J. M. D. *Langmuir* **2008**, *24*, 10560.
39. Wang, G. X.; Wang, B.; Park, J.; Yang, J.; Shen, X. P.; Yao, J. *Carbon* **2009**, *47*, 68.
40. ASTM Standard D 4187. *ASTM.* **1985**.
41. O'Brien, R. W.; Midmore, B. R.; Lamb, A.; Hunter, R. J. *Faraday Discuss. Chem. Soc.* **1990**, *90*, 301.
42. Gao, H. J.; Zhang, S. H.; Lu, F.; Jia, H.; Zheng, L. Q. *Colloid. Polym. Sci.* **2012**, *290*, 1785.
43. Teng, C. C.; Ma, C. C. M.; Lu, C. H.; Yang, S. Y.; Lee, S. H.; Hsiao, M. C.; Yen, M. Y.; Chiou, K. C.; Lee, T. M. *Carbon* **2011**, *49*, 5107.
44. Hsiao, S. T.; Ma, C. C. M.; Tien, H. W.; Liao, W. H.; Wang, Y. S.; Li, S. M.; Huang, Y. C. *Carbon* **2013**, *60*, 57.
45. Li, D.; Muller, M. B.; Gilje, S.; Kaner, R. B.; Wallace, G. G. *Nat. Nanotechnol.* **2008**, *2*, 101.
46. Ren, L. L.; Liu, T. X.; Guo, J.; Guo, S. Z.; Wang, X. Y.; Wang, W. Z. *Nanotechnol.* **2010**, *21*, 335701.
47. Choi, E. Y.; Han, T. H.; Hong, J.; Kim, J. E.; Lee, S. H.; Kima, H. W.; Kim, S. O. *J. Mater. Chem.* **2010**, *20*, 1907.
48. Gao, J. F.; Hu, M. J.; Dong, Y. C.; Li, R. K. Y. *ACS. Appl. Mater. Inter.* **2013**, *16*, 7758.
49. Kuilla, T.; Bhadra, S.; Yao, D.; Kim, N. H.; Bose, S.; Lee, J. H. *Prog. Polym. Sci.* **2010**, *11*, 1350.
50. Lee, K. H.; Hong, J. H.; Kwak, S. J.; Park, M.; Son, J. G. *Carbon* **2015**, *83*, 40.